small methods
www.small-methods.com

Cascading Photoelectric Detecting and Chemiresistive Gas-Sensing Properties of $Pb_5S_2I_6$ Nanowire Mesh for Multi-Factor Accurate Fire Alarm

Gui-Qian Huang, Ying-Xue Jin, Shao-Zhen Luo, Zhi-Hua Fu, Guan-E Wang, and Gang Xu**

Accurate fire warning is very important for people's life and property safety. The most commonly used fire alarm is based on the detection of a single factor of gases, smoke particles, or temperature, which easily causes false alarm due to complex environmental conditions. A facile multi-factor route for fabricating an accurate analog fire alarm using a $Pb_5S_2I_6$ nanowire mesh based on its photoelectric and gas-sensing dual function is presented. The $Pb_5S_2I_6$ nanowire mesh presents excellent photoelectric detection capabilities and is sensitive to ppm-level NO_2 at room temperature. Under the "two-step verification" circuit of light and gas factors, the bimodal simulation fire alarm based on this $Pb_5S_2I_6$ nanowire mesh can resist the interference of complex environmental factors and effectively reduce the false alarm rate.

1. Introduction

Fires are the most frequent and common disaster that threaten public safety and social development.[1] Every year, the number of deaths caused by fires is 20 times those caused by hurricanes, tornadoes, floods, and earthquakes altogether. For instance, in China, about 250 000 fires were reported in 2020. These fires resulted in 1183 civilian fire fatalities, 775 civilian fire injuries, and an estimated $4 billion direct property loss. The occurrence of fire is usually accompanied by the generation of harmful gases, smoke particles or high temperature. Fire alarms are based on the detection of the change of these factors.[2] However, traditional alarms are designed to detect only one of the above factors. These alarms are easily be disturbed, thereby delivering false alarm; disturbance is caused by environmental factors, such as cigarette smoke, welding, dust, humidity, and so on.[3] Frequent false positives will reduce public confidence and waste public resource. The detection of fires accurately by a single-factor fire alarm is still a big challenge.

Compared with single-factor detection, multi-factor detection is an effective way to improve the reliability and can effectively reduce false alarm rate.[4] The most commonly used approach is to combine several types of single-factor sensors into one alarm. However, the complicated integration technology and cumbersome calculations of multi-factor detection increase the manufacturing cost.[5] Moreover, the integration of multiple devices will increase the size of devices, which is not conducive to miniaturization. Thus, the simultaneous detection and high selectivity of multi-complex stimuli from the ambient environment remain a challenge. A feasible strategy to solve the above issues is to create a multifunctional sensing material that can provide multi-factor detection. However, to our best knowledge, no report on multi-factor detection of gas and light with one device for fire alarm has been published.

To solve the above problems, we designed and fabricated a semiconductor based on chemiresistive sensors, which are promising as multi-factor detectors due to their low fabrication cost, smooth operation, and potential for miniaturization.[6] Notably, by applying the advantage of semiconductors, for example, their resistance is sensitive to not only environmental gas but also to light,[7] it is possible to design a "two-step verification" circuit to realize the monitoring of light and gas synchronously. In this work, we constructed a photoelectric and gas-sensing dual-function sensor with $Pb_5S_2I_6$ nanowire mesh for the development of an analog fire alarm device. $Pb_5S_2I_6$

G.-Q. Huang, Y.-X. Jin, S.-Z. Luo, Z.-H. Fu, G.-E. Wang, G. Xu
State Key Laboratory of Structural Chemistry
Fujian Institute of Research on the Structure of Matter
Chinese Academy of Sciences
Fuzhou, Fujian 350002, China
E-mail: gewang@fjirsm.ac.cn; gxu@fjirsm.ac.cn
Y.-X. Jin
University of Chinese Academy of Sciences (UCAS)
Beijing 100049, China
S.-Z. Luo
College of Chemistry and Materials Science
Fujian Normal University
Fuzhou, Fujian 350007, China
G. Xu
Fujian Science and Technology Innovation Laboratory
for Optoelectronic Information of China
Fuzhou, Fujian 350108, China
G. Xu
Key Laboratory of Advanced Energy Materials Chemistry
(Ministry of Education)
College of Chemistry
Nankai University
Tianjin 300071, China

The ORCID identification number(s) for the author(s) of this article can be found under https://doi.org/10.1002/smtd.202200470.

DOI: 10.1002/smtd.202200470

nanowire mesh film was prepared on the solid–liquid interface through a substrate-assisted synthesis. Compared with its bulk counterpart, $Pb_5S_2I_6$ nanowire mesh had a much larger surface area and hierarchical nanostructure for fast mass transport and an efficient 1D pathway for charge transport, which endowed it with excellent photodetection/gas-sensing performances. Based on these properties, a "two-step verification" circuit was designed and applied to simulate fire detection. Besides the response of gases, smoke was another factor produced by fire that can be further judged by the photoelectric response of smoke to the refraction of the built-in light source. A true fire will be judged only when the gas responses and light responses exist together. Under the dual detection of smoke and gas factors, this bimodal simulation fire alarm can interfere with complex environmental factors and effectively reduce the false alarm rate. This is the first time that a single material that combines photoelectric detection and gas sensing has been used as an analog fire alarm device.

2. Results and Discussion

For photodetection and gas sensing, a large-area high-quality film increased the specific area and promoted the capture and adsorption of gas molecules, which had a significant impact on photoconductivity and gas sensing. Inspired by that, $Pb_5S_2I_6$ nanowire mesh was synthesized by the reaction of isothiocyanate and PbI_2 in hydrothermal condition. Unlike the reported sulfur sources, the slow release of S^{2-} from isothiocyanate synthesized large-area nanowire films, which can spontaneously form at the liquid–solid interface (**Figure 1**a). In the structure of $Pb_5S_2I_6$, the Pb atoms were coordinated by μ_3- and μ_2-bridging I atoms to form a 3D open framework of Pb_3I_6. The Pb_2S_2 chains were accommodated in the channels through Pb–I covalent bond (Figure 1b). $Pb_5S_2I_6$ nanowires with a diameter of about 100 nm were interwoven to form the self-assembled mesh with a multi-channel structure, as shown in Figure 1c. Such a morphology provides a high surface area to volume ratio, which may be conducive to photoelectric and gas-sensitive responses. Selected area electron diffractions (SAED) of the $Pb_5S_2I_6$ nanowire matched the monoclinic system, further confirming the crystalline phase and purity of $Pb_5S_2I_6$ (Figure S1, Supporting Information). The powder X-ray diffraction pattern (PXRD) analyzed the crystalline phase of the $Pb_5S_2I_6$ nanowire, and no impurities were detected (Figure 1d). The $Pb_5S_2I_6$ nanowire is a p-type semiconductor (Figure S2, Supporting Information) with a band gap of 2.01 eV (Figure 1e), as judged by UV–vis absorption and ultraviolet photo-electron spectroscopy. The semiconductor property of $Pb_5S_2I_6$ nanowires was measured to the compressed pellets by the two-terminal direct current method at different temperatures. The conductivity of the sample was 3×10^{-12} S cm^{-1} at room temperature, and it increased with the increasing temperature (Figure S3, Supporting Information), thereby showing its typical semiconductor characteristics.

Photodetectors can convert light signals to electrical signals and are extensively studied in the fields of image sensing, optical communication, environmental monitoring, and space detection.[8] Recently, the photodetection performance of $Pb_5S_2I_6$ single crystal or nanowire morphology has been reported.[9] To study the photoelectric properties of the $Pb_5S_2I_6$ nanowire mesh, this nanowire mesh was transferred to the interdigital electrode (Figure S4, Supporting Information).

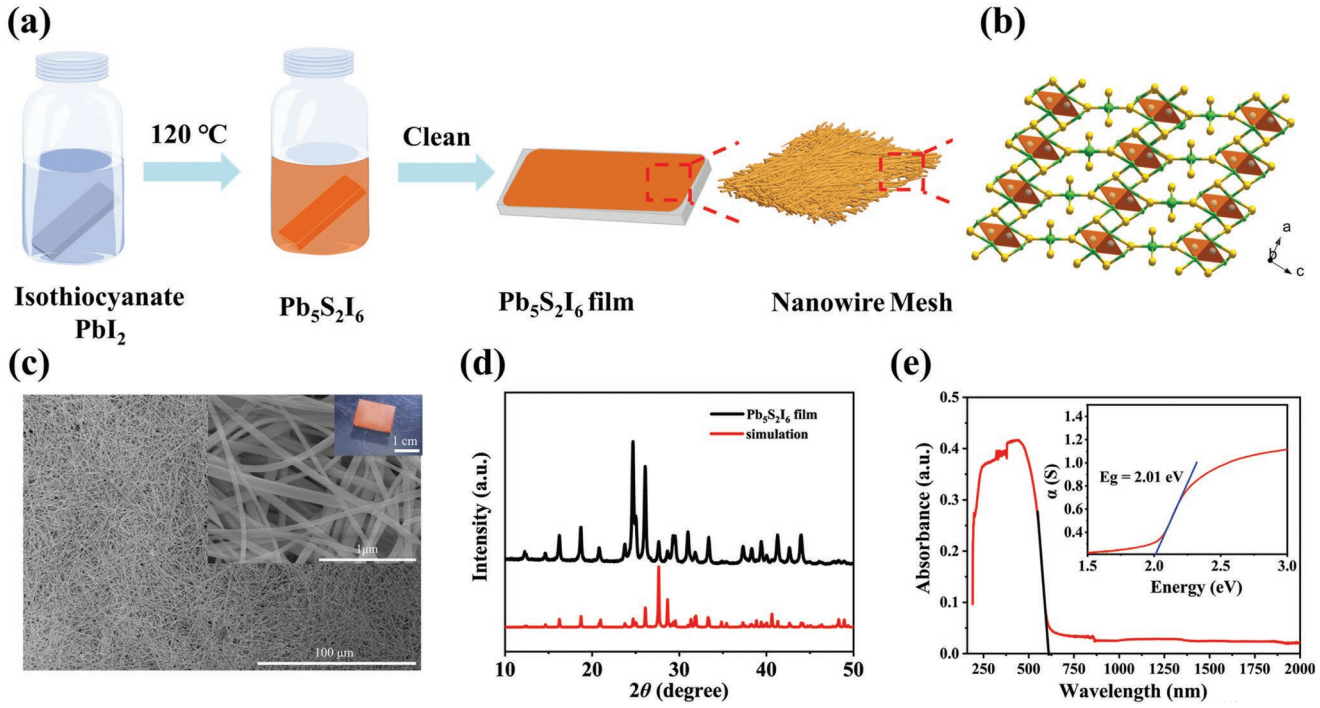

Figure 1. Characterization of the $Pb_5S_2I_6$ nanowire. a) Synthesis of $Pb_5S_2I_6$ nanowire mesh. b) Structure of $Pb_5S_2I_6$ viewed along the *b* axis. c) Scanning electron microscopy (SEM) image of $Pb_5S_2I_6$ nanowire mesh. d) XRD diffraction pattern of $Pb_5S_2I_6$ nanowires. e) UV–vis absorbance spectrum of $Pb_5S_2I_6$ nanowires. Inset is the corresponding K–M transformation of UV–vis absorption spectrum.

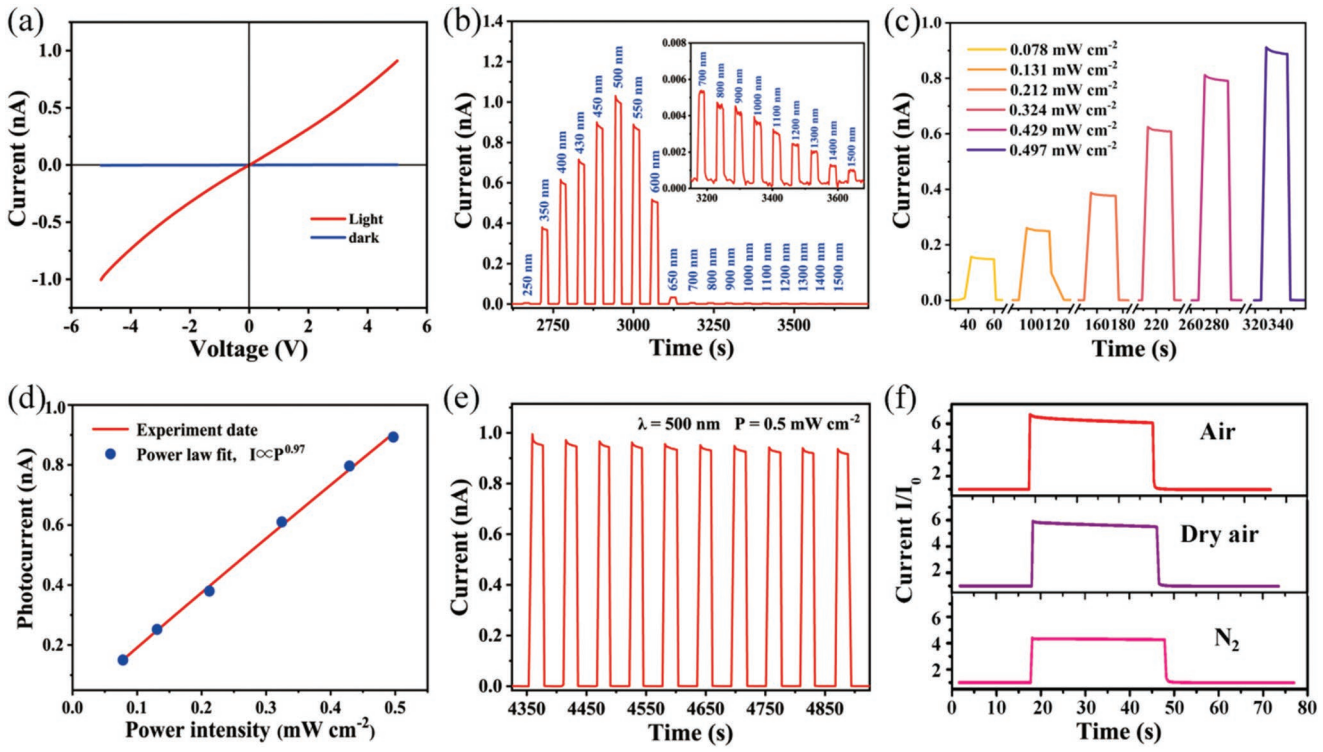

Figure 2. Optoelectronic performance of $Pb_5S_2I_6$ nanowire mesh. a) *I–V* characteristics of $Pb_5S_2I_6$ nanowire mesh under dark and light conditions. b) Wavelength-dependent photoresponse $Pb_5S_2I_6$ nanowire mesh (inset: enlarged view at 700–1500 nm). c) Photoresponse of $Pb_5S_2I_6$ nanowire mesh at different light intensities at 500 nm. d) Change of photocurrent with light intensity. e) Periodic photoresponse of $Pb_5S_2I_6$ nanowire mesh under 500 nm light. f) The photoresponse of $Pb_5S_2I_6$ nanowire mesh in air, dry air, and N_2, normalized by dark current I_0.

The current–voltage (*I–V*) curve of the nanowire mesh under light/dark conditions had obvious current changes (**Figure 2**a). As shown in Figure 2b, the current increased sharply when irradiated by monochromatic light of different wavelength, it showed obvious photocurrent response over a wide wavelengths. An obvious photocurrent response was shown over a wide wavelengths range of 250 to 1500 nm. The best wavelength sensitivity was at 500 nm. Light-intensity-dependent optoelectronic properties of $Pb_5S_2I_6$ nanowire mesh were also studied (Figure 2c). As shown in Figure 2d, the photocurrent was highly dependent on the light intensity, which was close to the ideal value of 1 and had an experimental exponent value of 0.97. Under periodic light pulses of 0.497 mW cm^{-2} at 500 nm, the maximum photocurrent within ten cycles was almost the same, indicating its excellent stability and repeatability (Figure 2e). $Pb_5S_2I_6$ nanowire mesh had a short rise response time (1.6 s) and fall time (1.25 s) (Figure S5, Supporting Information). In addition, $Pb_5S_2I_6$ nanowire mesh also showed a current on–off ratio of 2×10^3, responsivity (R_λ) of 0.5 mA W^{-1}, external quantum efficiency (EQE) of 1.1%, and detectivity of 2×10^{10} J under this condition (Figure S6, Supporting Information). Compared with the reported $Pb_5S_2I_6$ photoelectric performance, this nanowire mesh had the highest on–off ratio and detection rate. These results indicated that this $Pb_5S_2I_6$ nanowire mesh was expected to be used in photoelectric detection fields. The photoresponse of the $Pb_5S_2I_6$ nanowire mesh in various carrier gases was presented in Figure 2f. The photocurrent value was about 6.63 times larger than the dark levels in normal atmosphere, and the photoresponse value in dry air (I_{on}/I_{off} = 5.88) was comparable with that in normal atmosphere. In addition, this value decreased to four times in N_2. The adsorption of oxygen and hydroxyl (O_2^- from O_2, and OH^- from H_2O) on the surface of $Pb_5S_2I_6$ nanowire also played an important role in photocurrent response,[10] that led to the formation of an accumulation layer for $Pb_5S_2I_6$, with holes as the majority carriers. When the light radiated on the surface of the material, a large number of photo-generated electron–hole pairs were generated in the material, thereby increasing the photocurrent. Part of the photo-generated holes ran to the surface and compounded with oxygen negative ions and water negative ions to generate oxygen and water molecules. The concentrations of oxygen and water molecules were high in the normal air atmosphere, the reacted oxygen negative ions and water negative ions will be supplied by oxygen and water in the air. However, in a nitrogen environment, the oxygen and water adsorption were inhibited because of the low concentration of oxygen and water molecules. The photo-generated holes oxidized the adsorbed negatively charged oxygen and water ions on the surface, the concentration of photogenic holes decreased due to the lack of timely replenishment of adsorbed oxygen and water molecules. As a result, the photocurrent in a nitrogen environment was not as high as that in air.

In chemiresistive detectors, the conductivity change caused by the reaction between the target gas and oxygen species adsorbed on the surface of the sensing material was the

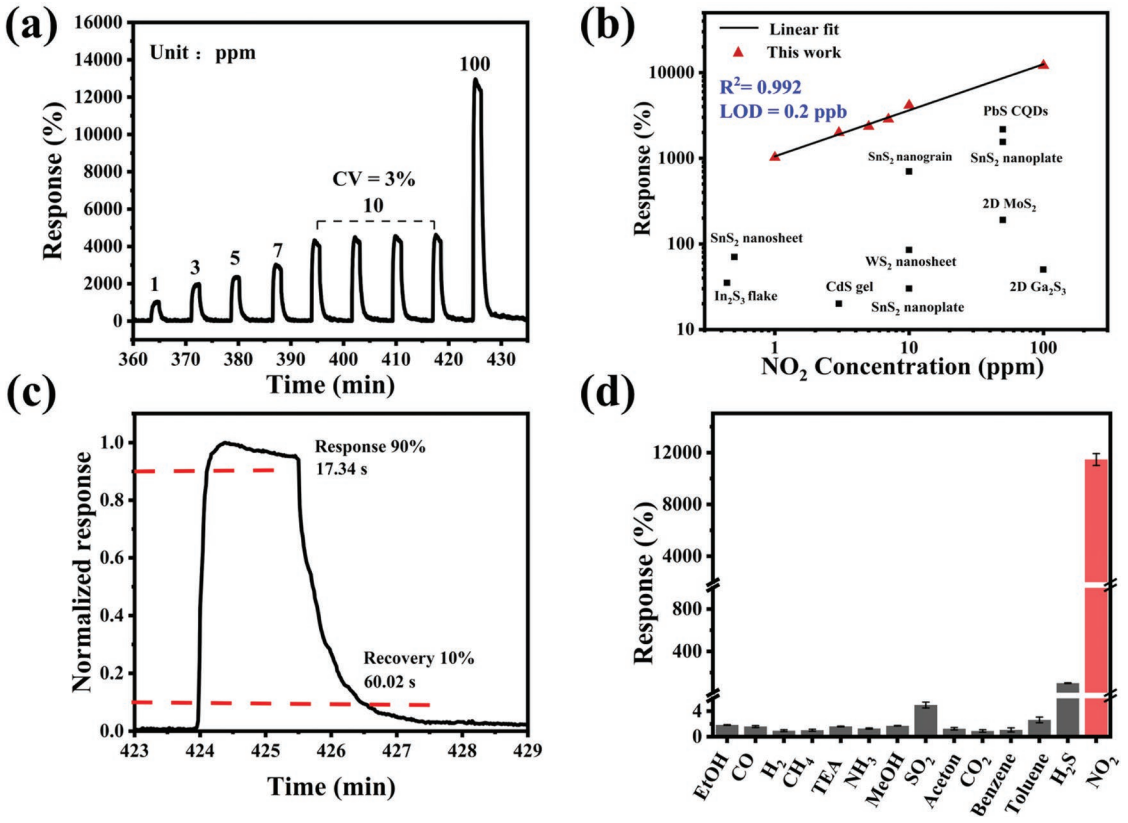

Figure 3. Gas-sensing performance of $Pb_5S_2I_6$ nanowire mesh. a) Response of $Pb_5S_2I_6$ nanowire mesh to different NO_2 concentrations at room temperature. b) Linear double logarithmic curve of the response and concentration of $Pb_5S_2I_6$ nanowire mesh and comparison with other pure metal sulfide materials at room temperature. SnS_2 nanograin,[11] SnS_2 nanosheet,[12] WS_2 nanosheet,[13] PbS CQDs,[14] SnS_2 nanoplate,[15] 2D MoS_2,[16] CdS gel,[17] SnS_2 nanosheet,[18] In_2S_3 flake,[19] and Ga_2S_3 nanosheet.[20] Data displayed in the graph are obtained or estimated from the corresponding cited reports. c) Response-recovery curve under 100 ppm NO_2. d) Column chart of responses toward different gases of $Pb_5S_2I_6$ nanowire mesh (concentration: 100 ppm).

basis of detection.[21] As tested in photoelectric properties, the adsorbed oxygen species on the surface of the $Pb_5S_2I_6$ nanowire mesh prompted us to study its gas sensitive properties. When $Pb_5S_2I_6$ nanowire mesh was exposed to NO_2 atmosphere, the current dramatically increased and reached saturation, and the response value was 12 000% under 100 ppm NO_2. As the sensor was exposed to dry air again, the resistance increased rapidly, and the current returned to the baseline. **Figure 3**a shows the dynamic response of the $Pb_5S_2I_6$ nanowire mesh at different concentrations of NO_2. The response coefficient of variation (CV) was 3% over four continuous cycles, indicating that $Pb_5S_2I_6$ nanowire mesh had good response repeatability to nitrogen dioxide. The log–log plot of response–concentration had a good linear relationship (R = 0.99) in the NO_2 concentration range of 1–100 ppm, which was useful for chemiresistive sensing (Figure 3b). Notably, compared with pure metal sulfide, the $Pb_5S_2I_6$ nanowire mesh showed the highest response to nitrogen dioxide (Figure 3b). The theoretical limit of detection (LOD) was 0.2 ppb by setting R = 10%, which was the lowest among pure metal sulfide chemiresistive sensing materials. To facilitate the judgment of the response speed level of the sensor performance, a single cycle process was normalized. The response time was set to 90% of the maximum current value, and the recovery time was set to 10% of the maximum current value. The response and recovery times were 17.34 and 60.02 s, respectively (Figure 3c). The responses of the $Pb_5S_2I_6$ nanowire mesh toward 100 ppm of typical 13 interference gases, including acetone, NH_3, benzene, CO_2, SO_2 and H_2S are shown in Figure 3d. It showed no response to these interference gases, indicating its high selectivity to NO_2 from other interference gases. These results indicate that the $Pb_5S_2I_6$ nanowire mesh had excellent gas-sensing properties at RT, which may be due to the large surface area and porous structure of the self-assembled mesh structure.

Nitrogen oxides (NO_x) come from the combustion of nitrogenous substances and are among the gaseous pollutants that cause atmospheric pollution.[6c,22] Fabricating a room temperature gas sensor for NO_x detection is still a great challenge.[23] The general commercial fire alarms that use photoelectric materials are utilized in monitoring the current change. The smoke particles produced by fires will scatter the built-in light to the photoelectric sensor, which causes current fluctuation. When the photocurrent exceeds the set limit, the fire alarm is triggered. However, environmental factors, such as dust, water mist, and other non-fire particles, easily interfere with this kind of alarm. Herein, we propose a new "two-step verification" circuit to realize the monitoring of light and gas synchronously, thereby avoiding the abovementioned interference and greatly improving the accuracy of the fire alarm (**Figure 4**).

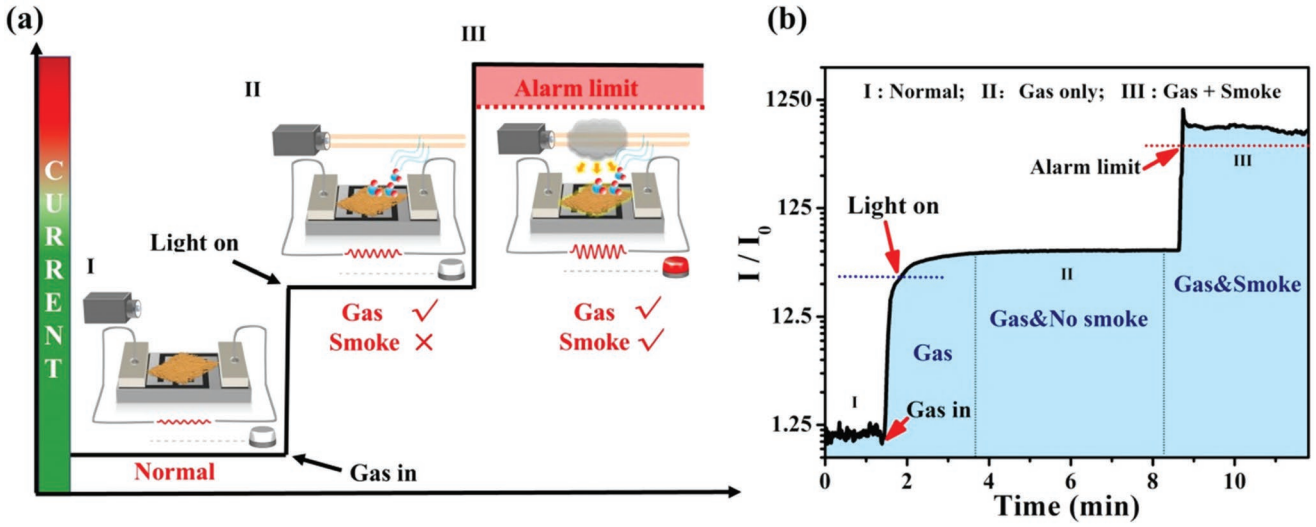

Figure 4. The "two-step verification" circuit for simulated fire alarm. a) Alarm mechanism diagram of bimodal sensor in a simulated fire environment. (I: Normal working state; II: Gas enters the alarm, and response current reaches the alarm limit for turning on the light. No smoke particle signals are received; it is not a real fire. III: Smoke enters the alarm, and the built-in light path is reflected by smoke particles on the photosensitive material; it is a real fire). b) The current of the bimodal sensor under the simulated fire environment.

The theoretical algorithm is based on the photoelectric and gas sensor properties of the $Pb_5S_2I_6$ nanowire mesh. As shown in Figure 4a, the current is at a relatively low level in a normal environment (I). With increasing concentration of the gas, the current will increase. When the current increases to the setting level, it will trigger the turning on of the light from the built-in power (II). At this time, there will be two cases, as follows. 1) It is a real fire, and the current will increase sharply for the light scattering of smoke particles. When the current reaches the setting level, the alarm will be triggered (III). 2) It is a non-fire condition, and the current will not further increase, because there are no smoke particles. For the double verification of light and gas, this bimodal sensor can greatly improve the accuracy of fire alarm.

To confirm our hypothesis, the $Pb_5S_2I_6$ nanowire mesh was used as simulation fire sensor in detail (Figure S7, Supporting Information). Figure 4b shows the working status of the $Pb_5S_2I_6$ bimodal sensor in a simulated fire environment. The current of $Pb_5S_2I_6$ film was $\approx 10^{-13}$ A in normal or only with interfering particles environment (I). The first step was to detect the gases. We used 10 ppm NO_2 to simulate the fire gas generated in a fire environment, which was less than the concentration of the gas when the fire started. The current is more than one order of magnitude higher than the normal value. The light was turned on as the current exceeded the light on setting value (II). The second step was to detect the smoke particles. There were two cases, as follows. 1) It was a false fire signal, and the current remained the same, because there were no smoke particles. 2) It was a real fire signal, and the current further increased (1 order) for the scattering of light by the smoke particles (III). When the current reached the alarm limit setting (red line), it triggered the fire alarm. This bimodal sensor effectively avoided the interference of other interferential particles and effectively improved the accuracy of commercial smoke alarms without complex integration technology. In addition, the material was stable in the environment. After 15 days, the response value toward NO_2 was unchanged (Figure S8, Supporting Information). To eliminate the interference of water vapor in the environment, the response of the material to nitrogen dioxide under different humidity levels was tested. The result showed that response value to nitrogen dioxide was larger than that in a pure relative humidity environment (Figure S9, Supporting Information). Thus, in practical applications, accurate NO_2 concentration needs to be corrected in different humidity accordingly in the future.

3. Conclusion

In summary, high-quality nanowire self-assembled $Pb_5S_2I_6$ nanowire mesh was successfully designed and prepared using hydrothermal condition at the liquid–solid interface. The $Pb_5S_2I_6$ nanowire mesh exhibited photoelectric and gas-sensing dual-function performance. It showed high on–off ratio (2×10^3) in the UV–vis region, fast rise/fall speed (1.6/1.25 s), high responsivity (0.5 mA W^{-1}), and high detectivity (2×10^{10} J). Meanwhile, it also exhibited high selectivity and high response to nitrogen dioxide at room temperature, which was the highest response (12 000%) to nitrogen dioxide sensing compared with pure metal sulfides. Furthermore, this was the first time that a single material can be used to determine the occurrence of fire through dual factors without integrated technology; thus, it can effectively reduce costs of alarms and improve alarm accuracy. This work proposed a new strategy for the construction of a new type of fire alarm, and provided the possibility for the preparation of a multi-factor fire alarm system for the accurate detection of fire in the future.

4. Experimental Section

Materials: All solvents and reagents were purchased without further purification. Lead iodide and stupid isothiocyanate were purchased from Adamas, ethanol (EtOH), methanol, acetonitrile, and *N*,*N*-dimethylformamide (DMF) were all derived from chemical reagents

Chinese medicine Holdings Limited, China. Ag–Pd interdigitated electrodes (the effective width: 7 mm, length: 4 mm, channel length:200 µm) were purchased from Beijing Elite Tech, Co. (China). Water was purified by mil-q purification system.

Preparation of $Pb_5S_2I_6$ Nanowire Mesh Film on Al_2O_3 Substrate: Lead iodide (0.018 g, 0.08 mmol) was added to an 8 mL glass bottle containing 6 mL of methanol solution, and 7 µL (0.04 mmol) of isothiocyanate was dropped. The treated substrate was placed in a bottle, followed by an ultrasonic water bath for 5 min, and then encapsulated in a 25 mL reactor. The $Pb_5S_2I_6$ nanowire mesh film was prepared by the reaction at 120 °C for 24 h and naturally cooled to room temperature.

Characterization: PXRD of the $Pb_5S_2I_6$ film sample was recorded on a Rigaku Miniflex 600 diffractometer (Cu $K\alpha$, λ = 1.540598 Å). The microscopic morphology of the film was observed by scanning electron microscopy (SEM, JEOL JSM-6700F). $Pb_5S_2I_6$ film was used for UV–vis diffuse reflectance spectra measurements operated on a Lambda 900 (PerkinElmer, USA). The electrical performance of the device was measured using a Keithley 4200 (USA) semiconductor characterization system.

Preparation of Multi-Function Sensor: The nanowire mesh film after the reaction was processed and cleaned. The substrate was taken out of the vial and then immersed in the DMF solution to wash the excess PbI_2, washed by ethanol to clean the excess ligand. The cleaned $Pb_5S_2I_6$ nanowire mesh film was transferred to a beaker filled with ethanol and shaken slightly in the solution. The film will fell off the Al_2O_3 substrate (Figure S10, Supporting Information). Then, the purchased Ag–Pd interdigital electrode was used to lift the film and air dried.

Measurement of Gas Sensor: The performance test of $Pb_5S_2I_6$-based gas sensor was carried out in a self-made device.[24] All tests were carried out at room temperature. $Pb_5S_2I_6$-based device was placed in a quartz tube with a stable gas flow rate of 600 mL min^{-1}, and under a bias of 5 V, the sensor test was performed by switching between dry air and standard gas. The Keithley 2602B sourcemeter was used to record the current change. The standard gas (Beijing Huayuan Co., Ltd.) and dry air (Xinhang Gas Co., Ltd.) used were both certified. The flow rate of the control gas was regulated by the mass flow controller (Beijing Qixing Qualiflow Electronic Equipment Manufacturing Co., Ltd. CS-200C).

Measurement of Photoelectric Detector: The $Pb_5S_2I_6$-based photodetector property assessment was performed on the Keithley 4200scs semiconductor parameter analyzer and Lakeshore probe station. All tests were carried out at room temperature. The bias voltage was set to 5 V, the vertical laser from Quanta Master fiber optic spectrometer was irradiated on the device, and a mechanical chopper was used to turn on and turn off the light irradiation.

Simulated Fire Environment Experiment Test: The simulated fire measurements were conducted by a home-made gas sensitivity test system (Figure S11, Supporting Information). A horizontal xenon lamp was placed above the quartz cavity as the built-in light source of the alarm. The smoke was produced by the smoke cake, and the smoke was filled in the airtight custom-made quartz cavity as the smoke produced during the fire. The $Pb_5S_2I_6$ bimodal sensor was placed in a closed quartz chamber of dry air with a steady flow rate (600 scc). After the current of the equipment was stabilized (5 V bias), 10 ppm of NO_2 was introduced as the harmful gas generated during the fire. After the gas response was saturated, the horizontal xenon lamp was turned on as the light source inside the alarm. The custom-made quartz cavity filled with smoke was placed in the horizontal light path (above the sensor), and the smoke reflected the light path to generate photocurrent.

Supporting Information

Supporting Information is available from the Wiley Online Library or from the author.

Acknowledgements

G.Q.H. and Y.X.J. contributed equally to this work. This work was supported by the National Natural Science Foundation of China (91961115, 22171263, 21975254, 22175176, and 21822109), the NSF of Fujian (2021J02017, 2020J01109, and 2022J06032), Youth Innovation Promotion Association CAS (2018342), and the Fujian Science & Technology Innovation Laboratory for Optoelectronic Information of China (2021ZR101).

Conflict of Interest

The authors declare no conflict of interest.

Data Availability Statement

The data that support the findings of this study are available in the supplementary material of this article.

Keywords

chemiresistive gas sensors, fire alarm, multi-factor detectors, optoelectronic materials

Received: May 12, 2022
Revised: June 9, 2022
Published online: June 22, 2022

[1] a) A. Gaur, A. Singh, A. Kumar, K. S. Kulkarni, S. Lala, K. Kapoor, V. Srivastava, A. Kumar, S. C. Mukhopadhyay, *IEEE Sens. J.* **2019**, *19*, 3191; b) X. Wang, H. Zhou, W. P. Arnott, M. E. Meyer, S. Taylor, H. Firouzkouhi, H. Moosmüller, J. C. Chow, J. G. Watson, *Fire Safety J.* **2020**, *113*, 102977.

[2] a) J. Fonollosa, A. Solorzano, S. Marco, *Sensors* **2018**, *18*, 553; b) K. Lee, Y. S. Shim, Y. G. Song, S. D. Han, Y. S. Lee, C. Y. Kang, *Sensors* **2017**, *17*, 303.

[3] B. A. Mueller, E. A. Sidman, H. Alter, R. Perkins, D. C. Grossman, *Inj. Prev.* **2008**, *14*, 80.

[4] a) Y. Chen, P. Lu, Z. Li, Y. Yuan, Q. Ye, H. Zhang, *ACS Appl. Mater. Interfaces* **2020**, *12*, 56604; b) C. Van Dyck, V. Geskin, A. J. Kronemeijer, D. M. de Leeuw, J. Cornil, *Phys. Chem. Chem. Phys.* **2013**, *15*, 4392.

[5] Q. Hua, J. Sun, H. Liu, R. Bao, R. Yu, J. Zhai, C. Pan, Z. L. Wang, *Nat. Commun* **2018**, *9*, 244.

[6] a) U. Yaqoob, M. I. Younis, *Sensors* **2021**, *21*, 2877; b) W. Ye, J. H. He, Q. Cao, W. J. Sun, J. Wang, Z. K. Chen, X. F. Cheng, C. Yu, J. M. Lu, *Adv. Mater.* **2021**, *33*, 2100674; c) S. Park, P. M. Bulemo, W.-T. Koo, J. Ko, I.-D. Kim, *Sens. Actuators, B* **2021**, *343*, 130137; d) J. Bai, Y. Shen, S. Zhao, Y. Chen, G. Li, C. Han, D. Wei, Z. Yuan, F. Meng, *Sens. Actuators, B* **2022**, *353*, 131191; e) Z. Meng, R. M. Stolz, L. Mendecki, K. A. Mirica, *Chem. Rev.* **2019**, *119*, 478; f) H. Y. Li, S. N. Zhao, S. Q. Zang, J. Li, *Chem. Soc. Rev.* **2020**, *49*, 6364; g) B. Liu, K. Li, Y. Luo, L. Gao, G. Duan, *Chem. Eng. J.* **2021**, *420*, 129881.

[7] V. Gupta, S. Sarkar, O. Aftenieva, T. Tsuda, L. Kumar, D. Schletz, J. Schultz, A. Kiriy, A. Fery, N. Vogel, T. A. F. König, *Adv. Funct. Mater.* **2021**, *31*, 2105054.

[8] Q.-Q. Huang, Y.-Z. Li, Z. Zheng, X.-M. Jiang, S.-S. Sun, H.-J. Jiang, W.-H. Deng, G.-E. Wang, T.-Y. Zhai, M.-D. Li, G. Xu, *CCS Chem* **2020**, *2*, 655.

[9] a) L. Sun, C. Wang, L. Xu, J. Wang, X. Chen, G.-C. Yi, *J. Mater. Chem. C* **2018**, *6*, 7188; b) H. Wang, G. Chen, J. Xu, Y. Xu, Q. Yang, *Cryst. Growth Des.* **2018**, *18*, 1987.

[10] a) K. Kirihara, K. Kawaguchi, Y. Shimizu, T. Sasaki, N. Koshizaki, K. Soga, K. Kimura, *Appl. Phys. Lett.* **2006**, *89*, 243121; b) C. L. Hsu,

H. H. Li, T. J. Hsueh, *ACS Appl. Mater. Interfaces* **2013**, *5*, 11142; c) L. Ge, S. Lei, A. H. Hart, G. Gao, H. Jafry, R. Vajtai, P. M. Ajayan, *Nanotechnology* **2014**, *25*, 335701.

[11] K. C. Kwon, J. M. Suh, T. H. Lee, K. S. Choi, K. Hong, Y. G. Song, Y. S. Shim, M. Shokouhimehr, C. Y. Kang, S. Y. Kim, H. W. Jang, *ACS Sens.* **2019**, *4*, 678.

[12] Z. Qin, K. Xu, H. Yue, H. Wang, J. Zhang, C. Ouyang, C. Xie, D. Zeng, *Sens. Actuators, B.* **2018**, *262*, 771.

[13] T. Xu, Y. Liu, Y. Pei, Y. Chen, Z. Jiang, Z. Shi, J. Xu, D. Wu, Y. Tian, X. Li, *Sens. Actuators, B.* **2018**, *259*, 789.

[14] H. Liu, M. Li, O. Voznyy, L. Hu, Q. Fu, D. Zhou, Z. Xia, E. H. Sargent, J. Tang, *Adv. Mater.* **2014**, *26*, 2718.

[15] Z. Yang, C. Su, S. Wang, Y. Han, X. Chen, S. Xu, Z. Zhou, N. Hu, Y. Su, M. Zeng, *Nanotechnology* **2020**, *31*, 075501.

[16] Y. Zhao, J. G. Song, G. H. Ryu, K. Y. Ko, W. J. Woo, Y. Kim, D. Kim, J. H. Lim, S. Lee, Z. Lee, J. Park, H. Kim, *Nanoscale* **2018**, *10*, 9338.

[17] C. C. Hewa-Rahiduwage, X. Geng, K. L. Silva, X. F. Niu, L. Zhang, S. L. Brock, L. Luo, *J. Am. Chem. Soc.* **2020**, *142*, 12207.

[18] K. Xu, N. Ha, Y. H. Hu, Q. J. Ma, W. J. Chen, X. M. Wen, R. Ou, V. Trinh, C. F. McConville, B. Y. Zhang, G. H. Ren, J. Z. Ou, *J. Hazard. Mater.* **2022**, *426*, 127813.

[19] K. Xu, B. Y. Zhang, M. Mohiuddina, N. Ha, X. M. Wen, C. H. Zhou, Y. X. Li, G. H. Ren, H. J. Zhang, A. Zavabetie, J. Z. Ou, *Nano Today* **2021**, *37*, 101096.

[20] M. M. Y. A. Alsaif, N. Pillai, S. Kuriakose, S. Walia, A. Jannat, K. Xu, T. Alkathiri, M. Mohiuddin, T. Daeneke, K. K. Zadeh, J. Z. Ou, A. Zavabeti, *ACS Appl. Nano Mater* **2019**, *2*, 4665.

[21] a) H. C. Ji, W. Zeng, Y. Q. Li, *Nanoscale* **2019**, *11*, 22664; b) C. P. Wang, C. Kashi, X. L. Ye, W. H. Li, G. E. Wang, G. Xu, *Chin. J. Struct. Chem.* **2021**, *40*, 1139; c) S. H. Sun, Q. C. Zhang, X. L. Ye, C. Kashi, W. H. Li, G. E. Wang, G. Xu, *Chin. J. Struct. Chem.* **2022**, *41*, 70; d) J. Z. Xiao, Z. H. Fu, G. E. Wang, X. L. Ye, G. Xu, *Chin. J. Struct. Chem.* **2022**, *41*, 2204054; e) D. Liu, Z. L. Tang, Z. T. Zhang, *Sens. Actuators, B* **2020**, *303*, 127114.

[22] a) S. W. Lee, H. G. Jung, J. W. Jang, D. Park, D. Lee, I. Kim, Y. Kim, D. Y. Cheong, K. S. Hwang, G. Lee, D. S. Yoon, *Sens. Actuators, B.* **2021**, *345*, 130361; b) J. Zeng, Y. Xu, J. Yu, X. Zhang, X. Zhang, H. Jin, Q. Jin, W. Shen, J. Zou, S. Deng, J. Jian, *ACS Sens.* **2019**, *4*, 2150; c) Z. Meng, R. M. Stolz, K. A. Mirica, *J. Am. Chem. Soc.* **2019**, *141*, 11929; d) Q. Liu, L. Gao, X. Su, F. Zhou, G. Duan, *Mater. Chem. Phys.* **2019**, *234*, 94; e) Y. Wang, L. Liu, F. Sun, T. Li, T. Zhang, S. Qin, *Front. Chem.* **2021**, *9*, 681313.

[23] a) J. Xuan, G. Zhao, M. Sun, F. Jia, X. Wang, T. Zhou, G. Yin, B. Liu, *RSC Adv.* **2020**, *10*, 39786; b) M. Liu, Y.-J. Chen, X. Huang, L.-Z. Dong, M. Lu, C. Guo, D. Yuan, Y. Chen, G. Xu, S.-L. Li, Y.-Q. Lan, *Angew. Chem., Int. Ed.* **2022**, *61*, e202115308; c) P. Shukla, P. Saxena, V. Bhatia, V. K. Jain, *Anal. Chim. Acta.* **2021**, *1177*, 338766; d) Y. Y. Wen, G. E. Wang, X. M. Jiang, X. Ye, W. H. Li, G. Xu, *Angew. Chem., Int. Ed.* **2021**, *60*, 19710; e) H. Mousavi, Y. Mortazavi, A. A. Khodadadi, M. H. Saberi, S. Alirezaei, *Appl. Surf. Sci.* **2021**, *546*, 149120; f) Y. Y. Liu, J. J. Liu, Q. J. Pan, K. Pan, G. Zhang, *Sens. Actuators, B* **2022**, *352*, 131001.

[24] M. S. Yao, W. X. Tang, G. E. Wang, B. Nath, G. Xu, *Adv. Mater.* **2016**, *28*, 5229.